

Audio2Gestures: Generating Diverse Gestures from Audio

Jing Li, Di Kang, Wenjie Pei, Xuefei Zhe, Ying Zhang, Linchao Bao, and Zhenyu He



arXiv:2301.06690v1 [cs.CV] 17 Jan 2023

Abstract—People may perform diverse gestures affected by various mental and physical factors when speaking the same sentences. This inherent one-to-many relationship makes co-speech gesture generation from audio particularly challenging. Conventional CNNs/RNNs assume one-to-one mapping, and thus tend to predict the average of all possible target motions, easily resulting in plain/boring motions during inference. So we propose to explicitly model the one-to-many audio-to-motion mapping by splitting the cross-modal latent code into shared code and motion-specific code. The shared code is expected to be responsible for the motion component that is more correlated to the audio while the motion-specific code is expected to capture diverse motion information that is more independent of the audio. However, splitting the latent code into two parts poses extra training difficulties. Several crucial training losses/strategies, including relaxed motion loss, bicycle constraint, and diversity loss, are designed to better train the VAE.

Experiments on both 3D and 2D motion datasets verify that our method generates more realistic and diverse motions than previous state-of-the-art methods, quantitatively and qualitatively. Besides, our formulation is compatible with discrete cosine transformation (DCT) modeling and other popular backbones (*i.e.* RNN, Transformer). As for motion losses and quantitative motion evaluation, we find structured losses/metrics (*e.g.* STFT) that consider temporal and/or spatial context complement the most commonly used point-wise losses (*e.g.* PCK), resulting in better motion dynamics and more nuanced motion details. Finally, we demonstrate that our method can be readily used to generate motion sequences with user-specified motion clips on the timeline.

Index Terms—Gesture, Motion generation, Cross-model generation

1 INTRODUCTION

Generating vivid human-like co-speech gestures is of great importance for producing attractive avatars that people are willing to interact with. There has been a surging demand for generating realistic human motions for given audio clips recently. However, this problem is very challenging because of the complicated one-to-many relationship between audio and motion. For example, a speaker may perform different gestures under different conditions (*e.g.* happy/peaceful mood, standing/sitting state, or different environments) when speaking the same words due to different mental and physical states.

Existing algorithms developed for audio to body dynamics have some obvious limitations. For example, [3] adapts a fully convolutional neural network to co-speech

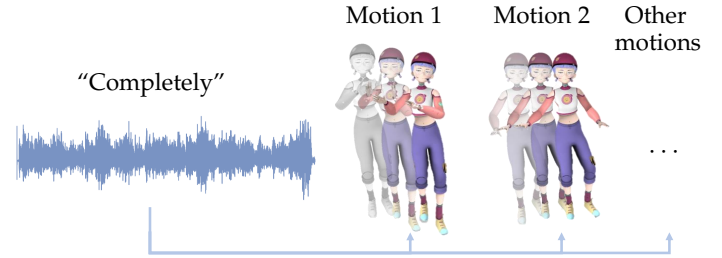


Fig. 1. Illustration of the existence of one-to-many mapping between audio and motion in Trinity dataset [1]. Different gestures are performed when the subject says “completely”. Similar phenomena broadly exist in co-speech gestures. The character used for demonstration is from Mixamo [2].

gesture synthesis tasks. Nevertheless, their model tends to predict averaged motion and thus generates motions lacking diversity. This is due to the underlying one-to-one mapping assumption of their model, which ignores that the relationship between speech and co-speech gesture is one-to-many in nature. Under such an overly simplified assumption, the model has no choice but to learn the averaged motion when several motions match almost the same audio clips in order to minimize the error. The above evidence inspires us to study whether or not explicitly modeling this multimodality improves the overall motion quality. To enhance the regression capability, we introduce an extra motion-specific latent code. With this varying *full* latent code, which contains the same shared code and varying motion-specific code, the decoder can regress different motion targets well for the same audio, achieving one-to-many mapping results. Under this formulation, the shared code extracted from audio input serves as part of the control signal. The motion-specific code further modulates the audio-controlled motion, enabling multimodal motion generation.

Although this formulation is straightforward, it is not trivial to make it work as expected. Firstly, there exists an easy degenerated solution since the motion decoder could utilize only the motion-specific code to reconstruct the motion. Secondly, we need to generate the motion-specific code since we do not have access to the target motion during inference. Our solution to the aforementioned problems is providing *random noise* to the motion-specific code so that the decoder has to utilize the deterministic information contained in the shared code to reconstruct the target.

But under this circumstance, it is unsuitable for forcing the motion decoder to reconstruct the exact original target

J. Li, W. Pei and Z. He are with Harbin Institute of Technology, Shenzhen.
D. Kang, X. Zhe, Y. Zhang and L. Bao are with Tencent AI Lab, Shenzhen.
L. Bao and Z. He are the corresponding authors.

motion anymore. So a *relaxed motion loss* is proposed to apply to the motions generated with random motion-specific code. Specifically, it only penalizes the joints deviating from their targets larger than a threshold. This loss encourages the motion-specific code to tune the final motion while respecting the shared code’s control.

A preliminary version of this work was presented in [4]. In this paper, we extend it from the following aspects: (1) We thoroughly investigate structured and perceptual metrics (*i.e.* STFT, SSIM, LPIPS, and FID) as training losses in our framework. We find them complementary to the previous point-wise losses since they additionally consider local temporal and/or spatial data structures. Especially with STFT, our network can consistently yield higher-quality motions. (2) We improve the user controllability by switching the latent space into discrete cosine transform (DCT) space, where different DCT components can control different dynamics of the generated motions. And we find the audio-motion shared code is more related to motion speed and rhythm while motion-specific code is more related to small range variations. (3) We conduct extensive ablation studies on different network backbones and hyper-parameters of motion losses and present more detailed discussions and analysis on the observations.

The overall contributions are summarized as follows:

- We present a co-speech gesture generation model whose latent space is split into audio-motion shared code and motion-specific code, to better model the training data pairs and generate diverse motions.
- We propose a new relaxed motion loss, accompanied by other training losses/strategies, to better avoid degeneration of the proposed network, enabling multimodal motion generation given the same audio input.
- The effectiveness of the proposed method has been verified on 3D and 2D gesture generation tasks by comparing it with several state-of-the-art methods. And this split formulation is compatible with DCT space modeling and other backbones (*i.e.* GRU, Transformer), and robust to hyper-parameter choice in the relaxed motion loss.
- In complement to the most commonly used point-wise metrics/losses, we analyze the generated motion by taking local spatial and/or temporal structure into consideration and introduce them as training losses to further improve the motion quality.
- As a byproduct, the proposed method is suitable for motion synthesis from annotations since it can well respect the predefined actions on the timeline by simply using their corresponding motion-specific code.

2 RELATED WORK

Audio to body dynamics. Early motion generation methods usually blend *motion clips/segments* chosen from a motion database according to hidden Markov model [5] or conditional random fields [6]. Algorithms focusing on selecting motion candidates from a pre-processed database usually cannot generate motions out of the database and does not scale to large databases. Recently, [7] extends this motion-matching based framework with a deep post-processing, where the retrieved motion clip using kNN

from the database is used as input to a conditional GAN to generate more diverse results. Rhythmic Gesticulator [8], which is also segment-based, generates gesture clip-by-clip via a VQ-VAE network to achieve better motion rhythm since its generator network is trained with motion clips segmented according to motion beats.

Recently, deep generative models (e.g. VAEs [9] and GANs [10]) have achieved great success in generating realistic images, as well as human motions [11], [12], [13]. For example, [14] utilizes a classic LSTM to predict the body movements of a person playing the piano or violin given the instrumental music. However, the body movements of a person playing the piano/violin show regular cyclic pattern and are usually constrained within a small pose space.

In contrast, generating co-speech gestures is more challenging in the following two aspects – the motion to generate is more difficult and the relationship between the speech and motion is more complicated. As a result, more powerfully networks are proposed and they often are trained with more data. For example, Speech2Gesture [3] proposes a more powerful fully convolutional network, consisting of a 8-layer CNN audio encoder and a 16-layer 1D U-Net decoder, to translate log-mel audio feature to gestures. HA2G [15] proposes to generate fine-grained gestures by associating the hierarchical feature between audio and motion. Speech2Gesture is trained with 14.4 hours of data per individual on average in comparison to 3 hours data in [14]. Other than greatly enlarged network capacity, the fully convolutional network also better avoids the error accumulation problem often faced by RNN-based methods. However, it still suffers from predicting the averaged motion due to the existence of one-to-many mapping in the training data. The authors further introduce adversarial loss and notice that the loss helps to improve diversity but degenerates the realism of the outputs.

In contrast, our method avoids learning the averaged motion by explicitly modeling the one-to-many mapping between audio and motion with the help of the extra motion-specific code. Similar to our split latent space formulation, DisCo [16] uses contrastive learning to disentangle the motion feature into motion rhythm and motion content.

Due to the lack of 3D human pose data, the above deep learning based methods [3], [14] have only tested 2D human pose data, which are 2D key point locations estimated from videos. Recently, [1] collects a 3D co-speech gesture dataset named Trinity Speech-Gesture Dataset, containing 244 minutes of motion capture (MoCap) data with paired audio, and thus enables deep network-based study on modeling the correlation between audio and 3D motion. This dataset has been tested by StyleGestures [17], which is a flow-based algorithm [17], [18]. StyleGestures generates 3D gestures by sampling poses from a pose distribution predicted from previous motions and control signals. However, samples generated by flow-based methods [17], [18] are often not as good as VAEs and GANs. In contrast, our method learns the mapping between audio and motion with a customized VAE. Diverse results can be sampled since VAE is a probabilistic generation model.

Human motion prediction. There exist many works focus on predicting future motion given previous motion [11], [12], [19]. It is natural to model sequence data with

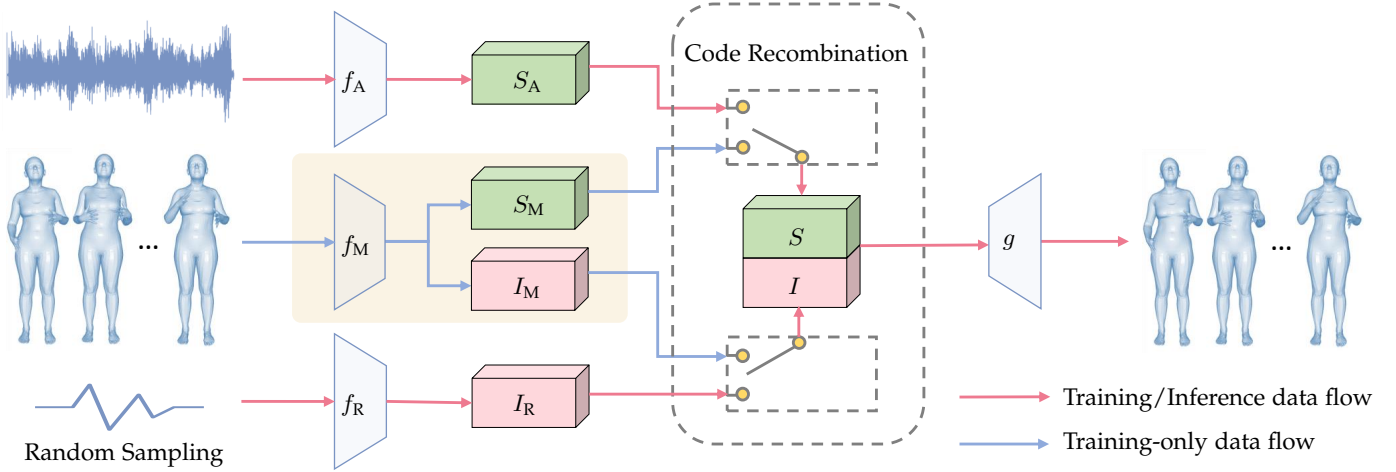


Fig. 2. Our method explicitly models the audio-motion mapping by splitting the latent code into shared and motion-specific codes. The decoder generates different motions by recombining the shared and motion-specific codes extracted from different sources. The data flow in blue is only used at the training stage because we do not have motion data during inference.

RNNs [11], [20], [21], [22]. But [12] has pointed out the RNN-based methods often suffer from error accumulation and thus are not good at predicting long-term human motion. So they propose to use a fully convolutional generative adversarial network and achieve better performance at long-term human motion prediction. Similarly, we also adopt a fully convolutional neural network since we need to generate long-term human motion. Specific to 3D human motion prediction, another type of error accumulation happens along the kinematic chain [19] because any *small* joint rotation error propagates to all its descendant joints, *e.g.* hands and fingers, resulting in *considerable* position error especially for the end-effectors (wrists, fingers). So QuaterNet [19] optimizes the joint position which is calculated from forward kinematics when predicting long-term motion. Differently, we optimize the joint rotation and position losses at the same time to help the model learn the joint limitation at the same time.

Multimodal generation tasks. Generating data with multimodality has received increasing interests in various tasks, such as image generation [23], [24], motion generation [25], [26]. For image generation, MUNIT [23] disentangles the embedding of images into content feature and style feature. BicycleGAN [24] combined cVAE-GAN [27] and cLRGAN [28], [29] to encourage the bijective consistency between the latent code and the output so that the model could generate different output by sampling different codes. For video generation, MoCoGAN [25] and S3VAE [26] disentangle the motion from the object to generate videos in which different objects perform similar motions. Different from [25], [26], our method disentangles the motion representation into the audio-motion shared information and motion-specific information to model the one-to-many mapping between audio and motion.

3 NETWORK OVERVIEW

The whole pipeline of our method is illustrated in Fig. 2. It is a conditional variational autoencoder (cVAE), with audio features as the condition (*i.e.* control signal) to generate co-speech gestures. Given an audio-motion pair $\{A, M\}$, the

latent code used to reconstruct the motion clip has been explicitly *split* into two parts (*i.e.* *shared* code S and *motion-specific* code I) to account for the frequently occurred *one-to-many* mapping between the *same* (technically, very similar) audio and many different possible motions.

Under this formulation, given the same audio input (resulting in the same shared code $S_A = f_A(A)$), varied motions produce different motion-specific code I_M through motion encoder f_M (*i.e.* $(S_M, I_M) = f_M(M)$), resulting in different *full* latent codes $(S_A \oplus I_M)$ so that the network can better model their relation from the audio-motion training pairs $(\hat{M} = g(S_A, I_M))$.

Since we do not have the target motion to extract I_M at inference time, a variational autoencoder [9] that allows latent space sampling is adopted to obtain a suitable motion-specific code I . During inference, shared feature S_A is extracted with f_A from the given audio A , serving as the control signal. Motion-specific feature I_R is generated with f_R from a randomly sampled signal. An additional mapping network is introduced empirically to facilitate its generation process. Finally, The co-speech gesture is generated by the decoder g that takes both S_A and I_R as input.

4 NETWORK TRAINING

In this section, we detail the training process, including commonly used newly introduced motion losses in Sec. 4.1 to help the network generate a valid pose, and our latent space learning losses/strategies in Sec. 4.2 to help the network to decouple the latent code into audio-motion shared and motion-specific code.

4.1 Motion learning

In this section, we will describe the losses introduced for better motion reconstruction. Our basic motion reconstruction loss (Sec. 4.1.1), which includes 3 most typically used individual loss terms, *i.e.* joint rotation, joint position, and joint speed losses at the same time. However, the motion reconstruction loss is a *point-wise* loss, which means the predicted motion is optimized frame-to-frame and joint-by-joint. This point-wise loss pays little attention to the

motion dynamics, thus easily resulting in averaged motion [3]. To help the network better model the motion dynamics, losses considering per-joint temporal dynamics (*i.e.* STFT in Sec. 4.1.2 and SSIM in Sec. 4.1.3) and a loss measuring abstract high-level similarity across different joints (*i.e.* LPIPS in Sec. 4.1.4) are introduced as a complement to the typical motion reconstruction loss. Their influences on the final generated motions are discussed in Sec. 6.2.3.

4.1.1 Motion reconstruction loss

We adopt the most commonly used motion losses as our basic *motion reconstruction loss*, including rotation loss, position loss, and speed loss. Formally, it is defined as follows:

$$L_{\text{mot}} = \lambda_{\text{rot}} \times L_{\text{rot}} + \lambda_{\text{pos}} \times L_{\text{pos}} + \lambda_{\text{speed}} \times L_{\text{speed}} \quad (1)$$

where λ_{rot} , λ_{pos} , λ_{speed} are weights. We detail each term in the following.

Angular distance, *i.e.*, geodesic distance, between the predicted rotation and the GT is adopted as the rotation loss. Mathematically,

$$L_{\text{rot}} = \frac{1}{J \times T} \sum_{j=1}^J \sum_{t=1}^T \cos^{-1} \frac{\text{Tr}(R_t^j (\hat{R}_t^j)^{-1}) - 1}{2} \quad (2)$$

Position loss is the L_1 distance between the predicted and target joint positions as follows:

$$L_{\text{pos}} = \frac{1}{J \times T} \sum_{j=1}^J \sum_{t=1}^T \|\hat{p}_t^j - p_t^j\|_1 \quad (3)$$

Speed loss is introduced to help the model learn the complicated motion dynamics. In our work, the joint speed v_t^j is defined as $v_t^j = p_{t+1}^j - p_t^j$. We optimize the predicted and target joint speed as follows:

$$L_{\text{speed}} = \frac{1}{J \times (T-1)} \sum_{j=1}^J \sum_{t=1}^{T-1} \|\hat{v}_t^j - v_t^j\|_1 \quad (4)$$

Our model can be trained with 2D motion data or 3D motion data. When modeling the 2D human motion, our method directly predicts the joint position. When modeling the 3D human motion, our method predicts the joint rotation and calculates the 3D joint positions with forward kinematics (FK). Concretely, the FK equation takes in as input the joint rotation matrix about its parent joint and the relative translation to its parent joint (*i.e.* bone length) and outputs joint positions as follows:

$$p_t^j = p_t^{\text{parent}(j)} + R_t^j s^j \quad (5)$$

where R_t^j represents the rotation matrix of joint j in frame t , p_t^j represents the position of joint j in frame t , s^j represents the relative translation of joint j to its parent, and $\text{parent}(j)$ represents the parent joint index of the joint j . We will always use j and t to index joints and frames in the following. Our model predicts joint rotation in 6D representation [30], which is a continuous representation that help the optimization of the model. The representation is then converted to rotation matrix R_t^j by Gram-Schmidt-like process, where R_t^j is the rotation matrix of joint j in frame t .

4.1.2 STFT

To help the network learn better temporal motion dynamics, we introduce Short-term Fourier transform (STFT) loss as a supervision signal. Following [31], the metric is calculated by:

$$L_{\text{stft}}(p, \hat{p}) = \frac{1}{T} \|\log |STFT(p; w, s)| - \log |(STFT(\hat{p}; w, s))|\|_1, \quad (6)$$

where w is the Hanning window of size 32 and the stride size s is set to 1/4 of the window size.

4.1.3 SSIM

Structural similarity index measure (SSIM) [32], which is originally proposed to measure the similarity between two images, considers local inter-dependencies among pixels. By treating joint number and frame dimensions as “image” height and width and xyz as channels, we can define the SSIM between two motions to measure their similarity with the consideration of local inter-dependencies (*i.e.* motion dynamics). Concretely, motion SSIM and the corresponding luminance l (*i.e.* averaged joint position), contrast c , and structure s are defined as follows.

$$SSIM(p, \hat{p}) = [l(p, \hat{p})]^\alpha \cdot [c(p, \hat{p})]^\beta \cdot [s(p, \hat{p})]^\gamma, \quad (7)$$

where l , c and s are calculated by:

$$l(p, \hat{p}) = \frac{2\mu_p \mu_{\hat{p}} + C_1}{\mu_p^2 + \mu_{\hat{p}}^2 + C_1} \quad (8)$$

$$c(p, \hat{p}) = \frac{2\sigma_p \sigma_{\hat{p}} + C_2}{\sigma_p^2 + \sigma_{\hat{p}}^2 + C_2} \quad (9)$$

$$s(p, \hat{p}) = \frac{\sigma_{p\hat{p}} + C_3}{\sigma_p \sigma_{\hat{p}} + C_3} \quad (10)$$

The μ_p ($\mu_{\hat{p}}$) is the average of joint positions across time:

$$\mu_p = \frac{1}{N} \sum_{t=1}^T p_t. \quad (11)$$

The σ_p is the standard deviation of the joint positions across time:

$$\sigma_p = \left(\frac{1}{N-1} \sum_{t=1}^T (p_t - \mu_p)^2 \right)^{\frac{1}{2}}. \quad (12)$$

The σ_{xy} is the covariance of the joint positions across time:

$$\sigma_{p\hat{p}} = \frac{1}{N-1} \sum_{t=1}^T (p_t - \mu_p)(\hat{p}_t - \mu_{\hat{p}}) \quad (13)$$

In our experiments, the α , β and γ are all set to 1. C_1 , C_2 and C_3 are set as 0.01^2 , 0.03^2 and $\frac{0.03^2}{2}$, respectively.

4.1.4 LPIPS

Learned perceptual image patch similarity (LPIPS) [33] measures the similarity between the generated motion and the groundtruth in feature space, which focuses on abstract high-level motion characteristics in complement to low-level joint-wise error, and has been used in many other generation tasks [34].

$$L_{\text{perceptual}} = \sum_l \frac{1}{T} \sum_{t=1}^T \|f_t^l - \hat{f}_t^l\|_2^2 \quad (14)$$

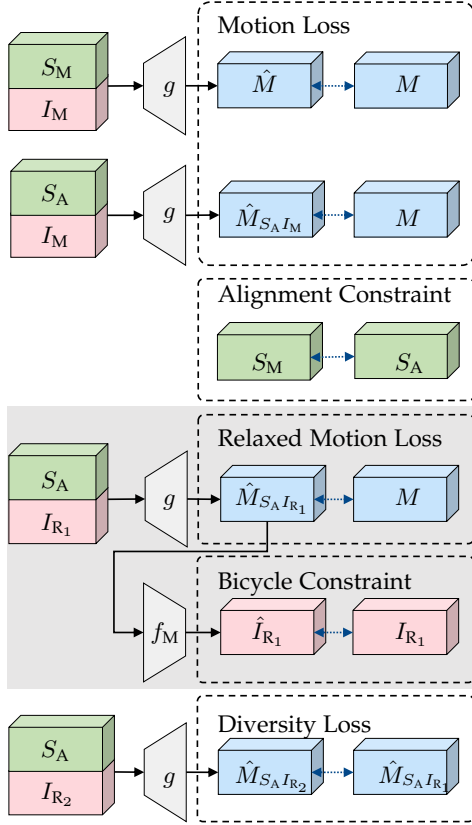


Fig. 3. The training details of our model. Our model is trained with alignment constraint, motion reconstruction losses, relaxed motion loss, bicycle constraint, diversity loss, and KL divergence. The alignment constraints and motion reconstruction loss help the model learn the audio-motion joint embedding. The relaxed motion loss avoids the degeneration of the shared code. The bicycle constraints and the diversity loss help reduce the mode-collapse problem and guide the model to generate multimodal motions. The KL divergence is omitted in the figure for the sake of brevity.

where f_t^l is the deep feature produced by the l^{th} residual block at t^{th} frame of the input motion.

Concretely, the network used to extract deep motion features is a convolutional autoencoder trained on Trinity Gesture dataset [1] using motion reconstruction loss in Eq. 1. The encoder and the decoder of the model consist of 5 residual blocks each [35] and take 6D joint rotation [30] as input and output. One residual block consists of two 1D dilated convolution layers. The final receptive field size of the motion encoder is 125 (frames).

4.2 Latent code learning

The shared code is expected to model the strong correlation between audio and motion while the motion-specific code is expected to capture diverse motion information more independent of the audio. So we need to 1) prevent any of S and I is ignored by the decoder (i.e. degenerate) and 2) encourage shared code S_A to contain more information and can be used interchangeably with S_M so that the audio input can effectively affect the output motion.

Shared code S is easily ignored by the motion decoder since motion AE is an easier task than cross modality translation. Thus, another data flow ($\hat{M}_{S_A I_R} = g(S_A, I_R)$, where I_R is from random noise.) is introduced so that the decoder

has to utilize the information contained in the shared code extracted from audio to reconstruct the target.

In total, five types of losses are introduced in addition to previous motion loss, including a shared-code *alignment constraint*, a *KL divergence* (omitted in the figure), a *relaxed motion loss*, a *bicycle constraint*, and a *diversity loss* (see Fig. 3). The *alignment constraint* and *relaxed motion loss* contribute to better learned joint embedding (i.e., shared code) of the audio and motion. The *relaxed motion loss* and *bicycle constraints* help avoiding degeneration (i.e. some part of the latent code is ignored and loses controllability on the final generated motion). The *bicycle constraints* and *diversity loss* are introduced to better model the multimodality of the motions. Detailed descriptions are in the following.

4.2.1 Shared code alignment

The shared code of paired audio and motion is expected to be the same so that we can safely use audio-extracted shared code during inference and generate realistic and audio-related motions. We align the shared code of audio and motion by the following alignment constraint:

$$L_{AC} = \|S_A - S_M\|_1. \quad (15)$$

4.2.2 KL divergence

During training, the distribution P of the latent code is constrained to match a target distribution Q with KL divergence as follows:

$$\mathcal{D}(Q(z) \| P(z|X)) = E_{z \sim Q} [\log Q(z) - \log P(z|X)], \quad (16)$$

where the X represents the input of the corresponding encoder (audio or motion in our case), and z represents its corresponding latent code. The above goal can be achieved by minimizing the Evidence Lower Bound (ELBO) [36]:

$$\log P(X|z) - \mathcal{D}[Q(z|X) \| P(z)]. \quad (17)$$

The second term of Eq. 17 is a KL-divergence between two Gaussian distributions (with a diagonal covariance matrix). The prior distribution P is set to Gaussian distribution (with a diagonal covariance matrix in our model, thus, the KL-divergence can be computed as:

$$\mathcal{D} = \frac{1}{2} \left(\text{tr}(\Sigma(X)) + \mu(X)^T \mu(X) - k - \log \det(\Sigma(X)) \right), \quad (18)$$

where k is the dimension of the distribution [36].

4.2.3 Degeneration avoidance

The motion decoder easily ignores the shared code input and solely use the motion-specific code to reconstruct the output motion (i.e. a motion auto-encoder) since it is a relatively easier task compared to audio2gestures that requires *translating* from one modality to another. This solution is a *degenerate* network, where the audio encoder is wasted and cannot control the final motion. Our solution to alleviating such degeneration is introducing an extra motion reconstruction task which takes shared code S_A extracted from the audio but random motion-specific code I_R as input. Ideally, the generated motion $\hat{M}_{S_A I_R}$ resembles its GT in some aspects but is not identical to its GT. In our case, we assume the generated poses are similar in the 3D world space. Thus we propose *relaxed motion loss*, which calculates

the position loss and penalizes the model only when the distance is larger than a certain threshold ρ :

$$L_S = \frac{1}{J} \sum_{i=1}^J \max(\|\hat{p}_i - p_i\|_1 - \rho, 0). \quad (19)$$

Recall that, to better model the relation between audio-motion pairs, we expect the existence of one-to-one correspondence (*i.e.* bijection) between the *full* latent code and the motion by introducing split latent spaces (*i.e.* shared latent code and motion-specific latent code). To encourage a bijection during training, we introduce bicycle constraint [24] (*i.e.* $M \rightarrow I \rightarrow M$ and $I \rightarrow M \rightarrow I$) to handle this mode-collapse problem. Since the motion reconstruction loss has already been introduced, an extra reconstruction loss of the motion-specific code is introduced as supplement:

$$L_{\text{cyc}} = \|\hat{I}_R - I_R\|_1 \quad (20)$$

4.2.4 Motion-specific code generation

By explicitly splitting the full latent code into two parts to handle the one-to-many mapping issue, the network could generate multimodal motions (*i.e.* motions in different types) using different and *appropriate* motion-specific codes. Although the motion-specific code could be sampled from Gaussian distribution directly, we noticed that the realism and diversity of the generated motions are not good. We hypothesize this is caused by the misalignment of the Gaussian distribution and the motion-specific code distribution. Thus, a mapping network is introduced to transform the signal sampled from Gaussian distribution to the motion-specific embedding. Concretely, we calculate the mean and variance for every channel and every sample of the I_M at the training stage. The sampled features will be fed into a mapping network, which is also a variational autoencoder, before concatenating them with the shared code to generate the final motions.

4.2.5 Motion diversification

To further encourage multimodality of the generated motion, a diversity loss [34], [37] is introduced.

$$L_{DS} = -L_{\text{pos}}(\hat{M}_{S M_{R_1}}, M). \quad (21)$$

Maximizing the diversity of the generated motions encourages the mapping network to explore the meaningful motion-specific code space. We follow the setting in [34] and directly maximize the joint position distance between two sampled motions since it is more stable than the original one [37].

5 DATASETS, EVALUATION, & IMPLEMENTATION DETAILS

In this section, we first introduce the datasets, evaluation metrics and implementation details separately in Sec. 5.1-5.3. Then we show the performance of our algorithm and compare it with three state-of-the-art methods 6.1. Finally, we analyze the influence of each module of our model on the performance by ablation studies 6.2. More results are presented in our project page¹.

1. <https://jingli513.github.io/audio2gestures>

5.1 Datasets

Trinity dataset. Trinity Gesture Dataset [1] is a large-scale speech to gesture synthesis dataset. This dataset records a male native English speaker talking many different topics, such as movies and daily activities. The dataset contains 23 sequences of paired audio-motion data, 244 minutes in total. We randomly split it into training set, which contains 19 sequences, and test set, which contains 4 sequences (*i.e.* NaturalTalking 01/25/27/30). All the training sequence frames are used for training and only the first 5000 frames of a test sequence are used for evaluation. The audio of the dataset is recorded at 44kHz. The motion data, consisting of 56 joints, are recorded at 60 frame per second (FPS) or 120 FPS using Vicon motion capture system.

S2G-Ellen dataset. The S2G-Ellen dataset, which is a subset of the Speech2Gesture dataset [3], contains positions of 49 2D upper body joint estimated from 504 YouTube videos, including 406 training sequences (469513 frames), 46 validation sequences (46027 frames), and 52 test sequences (59922 frames). The joints, which is estimated using OpenPose [38], include neck, shoulders, elbows, wrists, and hands.

5.2 Evaluation metrics

It is still an open problem to effectively measure the quality of the generated motions with objective metrics. In this paper, we measure the audio-driven gesture generation algorithms from three aspects, including similarity (Sec. 5.2.1), diversity (Sec. 5.2.2), and multimodality ((Sec. 5.2.3)).

5.2.1 Similarity metrics

Although the correlation between speech audio and co-speech gesture is as strong as that in talking face, certain patterns have been observed especially for *short-term* and *personalized* speech gesture generation scenario. Thus, similarity metrics are often adopted as an indicator to measure if the expected gestures have been generated.

Following Speech2Gesture [3], the L_1 distance of joint position in Eq. 22 and the percentage of correct keypoints (PCK) in Eq. 24 are adopted to evaluate the correlation between the generated motion and the input audio.

However, both L_1 and PCK are low-level point-wise losses computing similarity joint-by-joint and frame-by-frame, resulting in very different rankings from human perception. For example, it has been noticed that static motion (*e.g.* mean pose of the dataset) sometimes could also achieve a good L_1 and PCK performance [3]. So we additionally introduce several structural metrics to consider spatial and temporal similarities as complements, including short-term Fourier transform (STFT), structural similarity index measure (SSIM) [32], learned perceptual image patch similarity (LPIPS) [33], and Fréchet inception distance (FID).

L_1 distance is the average joint position error between corresponding joints between prediction \hat{p} and GT p :

$$L_1 = \frac{1}{T \times J} \sum_{t=1}^T \sum_{j=1}^J \|\hat{p}_t^j - p_t^j\|_1 \quad (22)$$

Note that the metric is comparable across different methods only if the same skeleton is used (*e.g.* larger skeleton corresponding to larger L_1 difference). We recommend normalize

according to wrist-to-wrist distance if different skeletons are used in different methods. For our skeleton, the wrist-to-wrist distance is 120.64 cm.

$$L_1^* = L_1 * \frac{l^*}{l^{curr}} \quad (23)$$

where l^{curr} is the wrist-to-wrist length of the used skeleton and l^* is the wrist-to-wrist length of a reference skeleton.

Percentage of correct keypoints (PCK) metric calculates the percentage of correctly predicted keypoints, where a predicted keypoint is thought correct if its distance to its target is smaller than a threshold δ :

$$L_{PCK} = \frac{1}{T \times J} \sum_{t=1}^T \sum_{j=1}^J \mathbf{1}[\|p_t^j - \hat{p}_t^j\|_2 < \delta], \quad (24)$$

where $\mathbf{1}$ is the indicator function and p_t^j indicates joint j 's position of frame t . The threshold δ is set to 0.2 in our experiments as in [3].

Short-term Fourier transform (STFT) is used to compare the motion dynamics between the generated motion and the groundtruth (Eq. 7, Sec. 4.1.3). In our experiments, the window size and stride size and FFT size of the STFT are set as 32 and 8 respectively (i.e. 1.06/0.265 sec for 30 FPS motion). This metric is similar with PSKL [12] when the window covers the entire motion sequence.

Structural similarity index measure (SSIM) measures the dynamics and the structure similarity at same time (Eq. 7, Sec. 4.1.3).

Learned perceptual image patch similarity (LPIPS) [33] measures the similarity between the generated motion and the groundtruth in a high-level feature space that considers both spatial and temporal information (Eq. 14, Sec. 4.1.4). The network used to extract this feature is trained with motion reconstruction task on Trinity dataset. We use the average pooled feature across time axis to represent a motion clip in LPIPS and FID calculation.

Fréchet inception distance (FID) [39] measures the similarity between a collection of generated motions and a collection of groundtruth motions by calculating the Fréchet distance on the extracted deep motion features. The deep features are extracted using the same network as LPIPS but only the output of the 4th residual block is used, which is then averaged across the temporal dimension. The final deep motion features is a 128 dimension vector. The Fréchet distance [39] is calculated by:

$$L_{FD} = \|\mu_1 - \mu_2\|^2 + \text{Tr}(\Sigma_1 + \Sigma_2 - 2(\Sigma_1 \Sigma_2)^{\frac{1}{2}}), \quad (25)$$

where μ and Σ is the mean and the variance of the motion features.

5.2.2 Diversity metric

Diversity measures how many different poses/motions have been generated within a long motion. People can easily notice the motion is not performed by a real person or get bored if only static motions or repeated motions can be generated. For example, RNN-based methods easily get stuck into some undesired static motion as the generated motion becomes longer and longer.

We first split the generated motions into equal-lengthed non-overlapping motion clips (50 frames per clip in our experiments) and we calculate diversity as the averaged L_1 distance of these short motion clips. Formally, it is defined as:

$$L_{Diversity} = \frac{1}{N \times \lceil N/2 \rceil} \sum_{a_1=1}^N \sum_{a_2=a_1+1}^N \|\hat{M}_{a_1} - \hat{M}_{a_2}\|_1 \quad (26)$$

where the \hat{M}_{a_1} and \hat{M}_{a_2} represent clips from the same motion sequence, N represents the count of the motion clips, which is $\frac{T}{50}$ in our experiments. Please note that jitter motion and invalid poses can also result in high diversity score, which means higher diversity is preferred only if the generated motion is natural.

5.2.3 Multimodality

Multimodality measures how many different motions could be sampled (through multiple runs) for a given audio clip. This is important due to the inherent one-to-many mapping between audio and motion. Note that multimodality calculates motion difference across different motions while diversity calculates the difference among short motion clips within the same long motion. We measure the multimodality by generating motions for an audio N times, which is 20 in our experiments, and then calculate the average L_1 distance of the motions.

$$L_{Multimodality} = \frac{1}{N \times \lceil N/2 \rceil} \sum_{a=1}^N \sum_{b=a+1}^N \|\hat{M}_a - \hat{M}_b\|_1 \quad (27)$$

where the \hat{M}_a and \hat{M}_b represent sampled motions generated through different runs for the same audio input. Similar to diversity, invalid motion will also result in abnormally high multimodality score.

5.2.4 User studies

We conduct user studies to analyze the visual quality of the generated motions since every metric measures only one aspect and they do not align well enough with human evaluations. Two use studies are conducted to compare 1) different methods and 2) to compare the newly introduced motion losses. For the first questionnaire, it contains four 20-second long videos. The motion clips shown in one video is generated by various methods from the same audio clip. The participants are asked to rank the motion clips from the following three aspects respectively:

- 1) Realism: which one is more realistic?
- 2) Diversity: which motion has more details?
- 3) Matching degree: which motion matches the audio better?

The results of the questionnaires are shown in Fig. 4. We show the count of different ranking in the figure. The average score of different metrics for each algorithm is listed after the corresponding bar. The scores assigned to each ratings are {5,4,3,2,1} for {best, fine, not bad, bad, worst} respectively.

For the second questionnaire, it contains 12 videos ranging in length from 10 seconds to 30 seconds. The motion clips shown in one video is generated by different methods (i.e. adding different motion losses from STFT, SSIM, or

LPIPS) given the same audio clip. The participants are asked to rank the motion clips according to the realism and diversity of the motion. The results of the questionnaires are shown in Fig. 6. We show the count of different ranking in the figure. The average score of different metrics for each algorithm is listed after the corresponding bar. The scores assigned to each ratings are {4,3,2,1} for {best, fine, not bad, worst} respectively.

5.3 Implementation details

5.3.1 Data processing

We detail the data processing of Trinity dataset and S2G-Allen dataset here.

Trinity dataset. The audio data are resampled to 16kHz for extracting log-mel spectrogram [40] feature using librosa [41]. More concretely, the hop size is set to SR/FR where SR is the sample rate of the audio and FR is the frame rate of the motion so that the resulting audio feature have the same length as the input motion. In our case, the resulting hop size is 533 since SR is 16000 and FR is 30. The dimension of the log-mel spectrogram is 64.

The motion data are downsampled to 30 FPS and then re-targeted to the SMPL-X [42] model. SMPL-X is an expressive articulated human model consisting of 54 joints (21 body joints, 30 hand joints, 3 face joints, respectively), which has been widely used in 3D pose estimation and prediction [42], [43], [44], [45]. The joint rotation is in 6D rotation representation [30] in our experiments, which is a smooth representation and could help the model approximate the target easier. Note that the finger motions are removed due to unignorable noise.

S2G-Allen dataset. Following [3], the data are split into 64-frame long clips (4.2 seconds). Audio features are extracted in the same way as the Trinity dataset. The 2D body joints are represented in a local coordinate frame relative to its root (*i.e.* origin is the root joint location) on the image plane.

5.3.2 Network

Most of our experiments take the TCN as the backbone of the encoders unless stated otherwise. Every encoder and decoder consists of 5 residual blocks [35], each containing several 1D convolution layers with ReLU non-linearity [46]. The residual block is similar to [47] except several modifications. Specifically, we use normal symmetric 1D convolutions that see both the history and the future instead of casual convolutions that see only the history. Similar to the bottleneck setting in the MLP-based autoencoders, the channel numbers of convolution layers are set to {128, 128, 96, 96, 64} for the audio encoder, {256, 256, 128, 128, 64} for the motion encoder, and {64, 128, 128, 256, 256} for the motion decoder. The kernel size (on time axis) of the convolution layers in backbones is 3. Two parallel 1×1 convolution layers are appended to the encoders to predict the mean and variance of the shared latent features. For non-variational case, only one 1×1 convolution layer is needed. The motion specific feature is sampled from Gaussian distribution, whose mean and variance is predicted from two parallel linear layers, respectively. Both the shared code and motion-specific code are set to 16 dimensions.

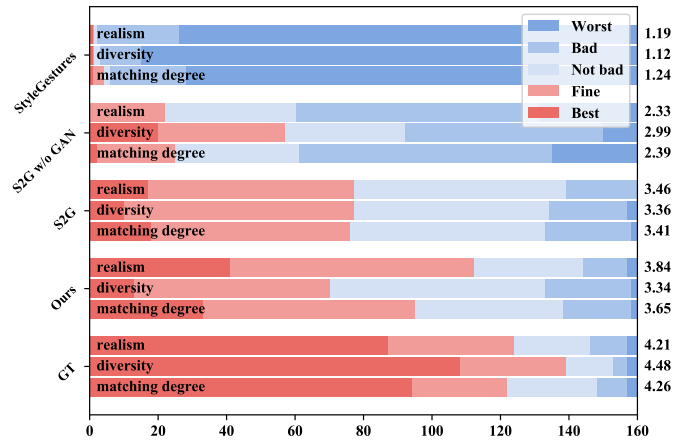


Fig. 4. User study results to compare our method against previous state-of-the-art methods. The horizontal axis represents the number of samples rated by the participants. In total, 160 comparisons have been rated (40 participants, 4 comparisons each questionnaire). Colored bars in different lengths indicate the counts of their corresponding rankings. The average score (higher is better) for each method is listed on the right. “S2G” is short for Speech2Gesture [3]. User study videos for comparison are provided in the supplementary. Also see Tab. 1 for quantitative evaluations.

5.3.3 Training

At the training stage, we randomly crop a 4.2-second segment of the audio and motion data, which is 64 frames for the S2G dataset (15 FPS) and 128 frames for the Trinity dataset (30 FPS). The model weights are initialized with the Xavier method [48] and trained 180K steps using the Adam [49] optimizer. The batch size is 32 and the learning rate is 10^{-4} . The λ_{rot} , λ_{pos} , λ_{speed} are set as 1, 1, 5 respectively, and ρ is set as 0.2 cm in our experiments. Our model is implemented with PyTorch [50].

6 RESULTS AND DISCUSSIONS

6.1 Comparison with state-of-the-art methods

We compare our method with two recent representative state-of-the-art methods, including one LSTM-based method named StyleGestures [51] and one CNN-based method named Speech2Gesture [3] on Trinity dataset. StyleGestures adapts normalizing flows [17], [18], [52] to speech-driven gesture synthesis. We train StyleGestures using the code released by the authors. The training data of the StyleGestures are processed in the same way as the authors indicate². Speech2Gesture, originally designed to map speech to 2D human keypoints, consists of an audio encoder and a motion decoder. Its final output layer has been adjusted to predict 3D joint rotations and is trained with the same losses as our method.

Quantitative experimental results are listed in Tab. 1 and user study results in Fig. 4. The results on Trinity show that our method outperforms previous state-of-the-art algorithms on the realism (see Fig. 4) and diversity metrics (see Tab. 1 and Fig. 4), demonstrating that it is beneficial to explicitly model the one-to-many mapping between audio and motion in the network structure.

2. The motions generated by StyleGestures are 20 FPS and have a different skeleton from our method. We upsample the predicted motion to 30 FPS and retarget it to SMPL-X skeleton with MotionBuilder.

TABLE 1

Comparisons with previous SOTA methods on Trinity dataset and S2G-Ellen dataset. \uparrow means the higher is better and \downarrow means the lower is better. For methods supporting sampling, we run 20 tests and report their *average* score and the *best* score (in parentheses). Speech2Gesture (“S2G” in the table) could not generate multimodality motions. See the accompanied video in our supplementary.

Dataset	Method	Pos. L_1 \downarrow	PCK \uparrow	Diversity \uparrow	Multimodality \uparrow
Trinity (3D)	S2G w/o GAN [3]	7.71	0.82	5.99	-
	S2G [3]	24.68	0.39	2.46	-
	StyleGestures [51]	18.97 (18.07)	0.34 (0.34)	2.34 (3.79)	7.55
	Audio2Gestures (Ours)	7.84 (7.65)	0.82 (0.83)	6.32 (6.52)	4.11
S2G-Ellen (2D)	S2G w/o GAN [3]	0.74	0.37	0.61	-
	S2G [3]	1.08	0.23	0.89	-
	Audio2Gestures (Ours)	0.94 (0.92)	0.33 (0.34)	0.84 (0.85)	0.77

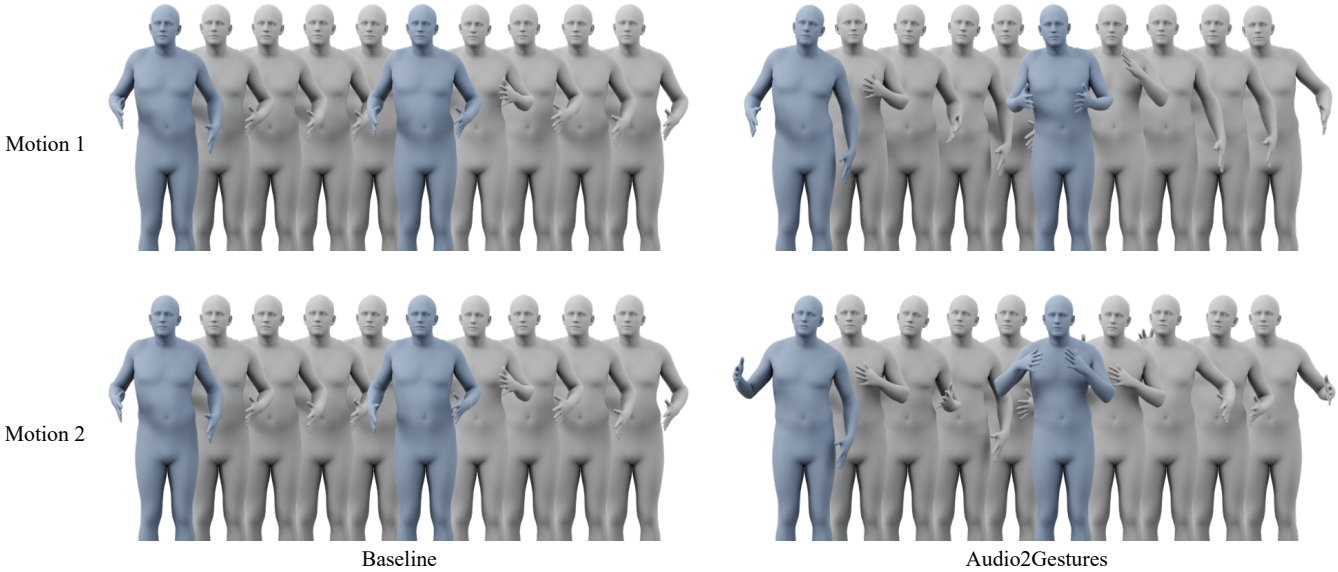


Fig. 5. Two examples (rows) of the generated multimodal motions given the same audio input using baseline method and our full method in Tab. 2. Two different motions generated by the baseline method have minimal difference since its multimodality score is only 0.41. In contrast, different motions predicted by our full model have certain similarity (e.g. lifting hands from waist) but not the same.

While StyleGestures supports generating different motions for the same audio via sampling, the quality of its generated motions is not very appealing (see Fig. 4). Also, its diversity score is the lowest, because LSTM output easily gets stuck into some fixed poses, resulting in long static motion afterwards. The algorithm is not good at generating long-term sequences due to the error accumulation problem of the LSTM. The LSTM-based StyleGestures has only been tested on up to 400-frame (13-second) long sequences originally. However, obviously deteriorated motions are generated when evaluating their algorithm to generate 5000-frame (166-second) long motions.

As for Speech2Gesture, the generated motions show similar realism with ours but obtain lower diversity score (Tab. 1) than our method. But Speech2Gesture does not support generating multimodal motions given the same audio input. Also note that Speech2Gesture with GAN generates many invalid poses and gets the worst performance. We have trained the model several times changing the learning rate range from 0.0001 to 0.01, and report the best performance here. The bad performance may be caused by the unstable of the training process of the generative adversarial network.

We also compare our method for 2D co-speech joint generation task on S2G-Ellen data [3] with Speech2Gesture [3],

which is originally designed for this 2D generation task. It can be seen that if GAN loss [10] is not used, the Speech2Gesture [3] model gets the best L_1 and PCK score but the worst Diversity performance, which is 0.61. We can clearly see the trade-off between better similarity metrics (i.e. L_1 , PCK) and the diversity metrics (i.e. diversity, multimodality). “S2G w/o GAN” achieves best similarity scores and worst diversity scores while “S2G” the opposite. In contrast, our method strikes a good balance between them.

6.2 Ablation study

In this section, we first verify the effectiveness of the proposed major modules in Sec. 6.2.1. Then we test the influence of different threshold values in the relaxed motion loss in Sec. 6.2.2. In Sec. 6.2.3, we study whether or not the introduced new motion losses can improve the quality of the generated motions. Finally, we conduct experiments to show that the proposed split formulation are applicable for different backbones in Sec. 6.2.4.

6.2.1 Modules

To gain more insights into the proposed components of our model, we test some variants of our model on the 3D Trinity dataset (Tab. 2). We run every variant 20 times and report

TABLE 2


Ablation study of the proposed components on the Trinity dataset. Note that every line adds a new component compared to its previous line, so the last line is our full A2G model. For methods supporting sampling, we run 20 tests and report their *average* score and the *best* score (in parentheses). See Fig. 6 for user study results and the accompanied video in our supplementary.

Method	Pos. L_1 ↓	Speed ↓	Acc. ↓	PCK ↑	STFT ↓	SSIM ↑	LPIPS ↓	FID ↓	Diversity ↑	Multimodality ↑
baseline	7.64 (7.63)	0.60 (0.60)	0.20 (0.16)	0.82 (0.82)	1.74 (1.74)	0.8765 (0.8766)	46.3 (46.3)	2.94 (2.93)	5.35 (5.37)	0.41
+ split	8.30 (7.86)	0.68 (0.63)	0.24 (0.18)	0.79 (0.82)	1.12 (1.11)	0.8567 (0.8665)	52.1 (48.6)	2.94 (2.16)	5.03 (6.09)	5.95
+ mapping net	7.73 (7.45)	0.67 (0.66)	0.24 (0.21)	0.81 (0.82)	1.11 (1.10)	0.8551 (0.8563)	47.8 (47.1)	2.19 (1.86)	6.13 (6.53)	3.59
+ bicycle constraint	7.69 (7.36)	0.64 (0.62)	0.24 (0.20)	0.82 (0.84)	1.14 (1.14)	0.8659 (0.8700)	46.3 (43.7)	2.16 (1.70)	6.35 (6.67)	3.99
+ diversity loss	7.86 (7.55)	0.67 (0.66)	0.24 (0.22)	0.81 (0.83)	1.13 (1.12)	0.8594 (0.8619)	48.6 (45.4)	2.22 (1.65)	6.58 (6.90)	4.10

TABLE 3

Influence of using different threshold ρ (in cm) in the relaxed motion loss for training. The best result of every metric is in bold and the second best result is underlined. MM represents multimodality. For easier comparison, we include their corresponding curves at the bottom, where the horizontal axis represents ρ from 0 to 5. We used $\rho = 0.2$ by default.

ρ	Pos. L_1 ↓	Speed L_1 ↓	Acc. L_1 ↓	PCK ↑	STFT ↓	SSIM ↑	LPIPS ↓	FID ↓	Diversity ↑	MM ↑
0	7.4421 (7.2117)	0.6345 (0.6163)	0.2315 (0.2059)	0.8403 (0.8541)	1.11 (1.10)	0.8679 (0.8720)	44.6 (42.8)	2.15 (1.80)	6.15 (6.45)	3.51
0.1	<u>7.6120</u> (7.3529)	<u>0.6295</u> (0.6235)	0.2259 (0.1919)	0.8208 (0.8329)	<u>1.11</u> (1.11)	0.8682 (0.8704)	46.3 (45.0)	2.25 (2.09)	6.20 (6.32)	2.70
0.2	<u>7.8613</u> (7.5515)	<u>0.6678</u> (0.6608)	0.2432 (0.2195)	0.8130 (0.8286)	1.13 (1.12)	0.8594 (0.8619)	48.6 (45.4)	2.22 (1.65)	<u>6.58</u> (6.90)	<u>4.10</u>
0.5	7.5915 (7.4267)	0.6509 (0.6378)	<u>0.2340</u> (0.2018)	0.8264 (0.8388)	1.09 (1.08)	0.8605 (0.8677)	46.2 (45.1)	2.06 (1.66)	<u>6.51</u> (6.74)	<u>3.33</u>
1	7.8480 (7.5192)	0.6688 (0.6494)	<u>0.2507</u> (0.2259)	0.8133 (0.8281)	1.15 (1.14)	0.8596 (0.8640)	47.2 (44.7)	<u>2.07</u> (1.66)	6.43 (6.60)	4.02
2	7.8575 (7.4219)	0.6561 (0.6402)	0.2428 (0.2062)	<u>0.8169</u> (0.8370)	1.14 (1.14)	0.8625 (0.8678)	46.8 (44.0)	<u>2.16</u> (1.59)	6.23 (6.66)	4.24
5	7.7102 (7.5064)	0.6631 (0.6353)	0.2523 (0.2063)	<u>0.8217</u> (0.8352)	1.16 (1.14)	0.8569 (0.8582)	<u>45.6</u> (44.8)	2.14 (1.80)	6.58 (7.16)	3.92



both *average* performance and the *best* performance (listed in parentheses). Note that the variation of our model comes from two different parts, the randomness introduced by the variational autoencoder and by the motion-specific feature sampling.

We start with a “baseline” model, which excludes the mapping net and the split code. It is trained with only the motion reconstruction losses (Eq. 1) and shared code constraint (Eq. 15). The average scores of Pos. L_1 , PCK, and diversity have little difference with their best scores, which indicates that the randomness of the VAE model alone have very little influence on generating multimodal motions.

The next setting is “+split”, which splits the output of the motion encoder into shared and motion-specific codes and introduces the relaxed motion loss (Eq. 19). This modification greatly improves the multimodality score by explicitly handling the one-to-many mapping (from 0.41 to 5.95), but it harms the similarity metrics (see “Pos. L_1 ”, “Speed”, “Acc.”, “PCK” and LPIPS). This huge performance drop might be caused by the misalignment between the sampled signal and the motion-specific feature. For example, we find a big difference in the statistics (*i.e.* the mean and variance) of the delta of motion-specific feature (between two consecutive frames) between the training samples and the randomly sampled one.

Thus, training set statistics and a StyleGAN fashion mapping network (“+mapping net”) are introduced to address the potential misalignment between the sampled signal and the real motion-specific feature automatically. The “+mapping net” model also outperforms the baseline model in the Pos., Speed, Acc., STFT, FID and Diversity metrics and gets a similar PCK metrics, but the model is able to generate multimodal motions.

Because generative models often suffer from mode collapse problem, two simple yet effective losses – the bicycle constraint (Eq. 20) and a diversity loss (Eq. 21) – are intro-

duced to alleviate the problem. Bicycle constraint improves the multimodality of the motions from 3.59 to 3.99. The diversity loss further improves the multimodality to 4.10 but has little influence on the similarity metrics.²

6.2.2 Thresholds in relaxed motion loss

In Tab. 3, we show the influence of the hyper-parameter ρ of the relaxed motion loss. When the threshold ρ is set to 0, the relaxed motion loss becomes the common L_1 loss, and the algorithm gets the best L_1 , PCK and LPIPS performance (7.42/0.83/44.2). As the ρ increases, the sampled motions are less penalized if they are not very similar to their corresponding groundtruth, resulting in gradually decreased performance with respect to similarity metrics. For example, the L_1 (LPIPS) error increases to 8.04 (0.79) and the PCK drops to 0.79 when ρ is set to 0.2. However, worse L_1 , PCK, and LPIPS performance do not necessarily mean the quality of the generated motion is not good due to the inherent weak and multimodal correlation between audio and motion especially for long-term motion synthesise. The FID is 1.66 when the $\rho = 0.2$ and is better than $\rho = 0$ whose FID is 1.81. What is more, the multimodality of the generated motion gradually getting better from 3.59 to 4.54, which indicates that more diverse motions could be generated given the same input audio (*i.e.* better multimodality).

6.2.3 Additional motion losses

We study the influence of three new motion losses (STFT, SSIM, and LPIPS) in Tab. 4. The basic motion reconstruction loss (Eq. 1) is always present.

These losses, in complement to commonly used point-wise losses in Eq. 1, measure the similarity of two motions with the consideration of spatial and/or temporal context.

They could also be viewed as relaxed motion losses from the perspective that they focus more on measuring the local structures aside from values point-by-point (*e.g.*

TABLE 4

Effect of introducing complementary motion losses. “+ loss_x” means including loss_x to “A2G + loss_x”. For methods supporting sampling, we run 20 tests and report their *average* score and the *best* score (in parentheses). Entries with improved performance are highlighted in blue. MM represents multimodality. See the accompanied video in our supplementary.

Basenet	Pos. L_1 ↓	Speed L_1 ↓	Acc. L_1 ↓	PCK ↑	STFT ↓	SSIM ↑	LPIPS ↓	FID ↓	Diversity ↑	MM ↑
A2G	7.8613 (7.5515)	0.6678 (0.6608)	0.2432 (0.2195)	0.8130 (0.8286)	1.13 (1.12)	0.8594 (0.8619)	48.6 (45.4)	2.22 (1.65)	6.58 (6.90)	4.10
+ STFT	7.9406 (7.6353)	0.6565 (0.6397)	0.2255 (0.1895)	0.8134 (0.8369)	1.02 (1.00)	0.8621 (0.8668)	49.8 (46.6)	2.88 (2.40)	5.06 (5.82)	4.88
+ SSIM	7.8623 (7.5101)	0.6384 (0.6239)	0.2211 (0.1803)	0.8167 (0.8326)	1.10 (1.09)	0.8647 (0.8694)	49.9 (45.2)	2.98 (2.37)	5.19 (6.09)	4.83
+ LPIPS	8.4157 (7.9884)	0.6680 (0.6147)	0.2521 (0.1836)	0.7895 (0.8132)	1.17 (1.16)	0.8551 (0.8683)	48.3 (43.5)	1.90 (0.95)	6.04 (6.86)	5.74
GT+ $\mathcal{N}(0,1)$	1.1617	1.2352	2.1369	1.00	2.78	0.8449	0.51	0.0004	10.1	-
GT+ $\mathcal{N}(0,5)$	4.4406	6.0598	10.503	0.99	4.06	0.2749	12.2	0.2001	11.7	-

L_1 distance), resulting in a trade-off between accuracy and quality (see the similarity metrics and other metrics in Tab. 4).

How to quantitatively measuring motion quality is an underdeveloped problem. The frame level metrics (Pos. L_1 , PCK) are widely used metrics, which are standard metrics of short-term motion prediction. However, the metrics are hard to reflect the performance of the long-term motion generation tasks, because of the audio-motion one-to-many mapping. For example, expressive ourselves with left hand or right hand have little difference in most occasions but have a large difference in Pos. L_1 score.

Another limitation is that the motion dynamics (e.g. smoothness) is one crucial factor that affects the user study results. However, we find the most commonly tested metrics (i.e. Pos. L_1 , PCK, and FID) can hardly tell whether the motion is smooth or jerky, and thus introducing speed, acceleration (Acc.), STFT, and SSIM as complements. To show their effectiveness, we add two levels of Gaussian noise to the Euler angles on every joint of the GT motion. Their results are listed in Tab. 4 for reference. Although the noisy motions jitter very much, Pos. L_1 , PCK, LPIPS, and FID are very insensitive to these obvious artifacts because Pos. L_1 , PCK completely do not consider temporal information and LPIPS and FID measure distance in high-level feature space, which might have ignored this low-level difference. In contrast, the Speed L_1 , Acc. L_1 , STFT, and SSIM can evaluate smoothness faithfully.

We notice that the motions predicted by the network trained with STFT loss usually contain more subtle motion details and they perform better on Speed, Acc., PCK, STFT, and SSIM metrics (from {0.6678/0.2432/0.8130/1.13/0.8594} to {0.6565/0.2255/0.8134/1.02/0.8621}). We conduct user study in Sec. 5.2.4 for qualitative evaluation. According to the feedback, using STFT as training loss indeed brings noticeable improvement from the perspective of motion quality.

When trained with SSIM loss, although the Pos., Speed, Acc., PCK, STFT, and SSIM metrics improve a lot ({7.8623/0.6384/0.2211/0.8167/1.10/0.8647}), no noticeable improvement has been observed according to the user study (Fig. 6).

LPIPS evaluates the similarity of the generated motion with the target motion in learned motion feature space instead of directly comparing the low level L_1 distance of joint position. Although the metric often corresponding well with the positional L_1 metric in our experiments, it

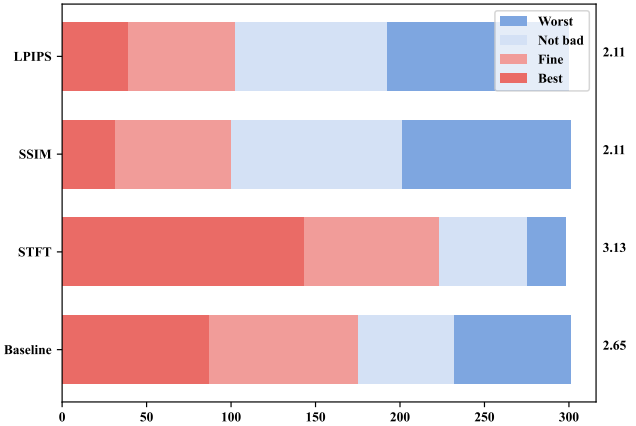


Fig. 6. User study results to compare the newly introduced motion losses. This user study specifically focus on the naturalness of the generated motion (i.e. no dedicated diversity and matching degree questions.) The horizontal axis represents the total number of samples rated by the participants. In total, 300 comparisons have been rated (25 participants, 12 comparisons each questionnaire). Colored bars in different lengths indicate the counts of their corresponding rankings. The average score for each row is listed on the right. User study videos for comparison are provided in the supplementary. Also see Tab. 4 for quantitative evaluations.

improves the multimodality of the generated motion a lot after adopted as a training loss, which raise to 4.68 from 3.57. Although the averaged Pos. L_1 and LPIPS drops to 8.33 and 48.3 from 7.84 and 47.0, the best performance of the metrics improved to 7.63 and 43.5. The FID and speed L_1 also better than the naive Audio2Gestures model.

6.2.4 Backbones

At the core of our Audio2Gestures is the split latent space and the strategies to better learn the latent codes. It does not require particular network architectures, so we study whether or not this formulation is applicable for other backbones, including GRU and Transformer, in this section. We replace the TCN backbone to extract latent codes with GRU-based [53] and Transformer-based [54] network and their results are listed in Tab. 5. Notice that the decoder to transform the latent codes to final motion remains unchanged in these experiments.

To make fairer comparisons, we use the same number of layers as the original TCN backbone. Concretely, the GRU backbone consists of 5 bidirectional GRU layers, each with 32 hidden neurons. The transformer backbone consists of 5 transformer encoder layers. The dimensions of the Q, K, and V of the self-attention layers are all set to 16, where Q, K,

TABLE 5

Comparisons of using different backbone networks. Trans. is short for Transformer. See the accompanied video in our supplementary.

Basenet	Pos. $L_1 \downarrow$	Speed $L_1 \downarrow$	Acc. $L_1 \downarrow$	PCK \uparrow	STFT \downarrow	SSIM \uparrow	LPIPS \downarrow	FID \downarrow	Diversity \uparrow	Multimodality \uparrow
baseline	7.64 (7.63)	0.60 (0.60)	0.20 (0.16)	0.81 (0.81)	1.74 (1.74)	0.8765 (0.8766)	46.3 (46.3)	2.94 (2.93)	5.35 (5.37)	0.41
A2G	7.86 (7.55)	0.67 (0.66)	0.24 (0.22)	0.81 (0.83)	1.13 (1.12)	0.8594 (0.8619)	48.6 (45.4)	2.22 (1.65)	6.58 (6.90)	4.10
A2G (GRU)	8.05 (7.77)	0.64 (0.64)	0.23 (0.22)	0.80 (0.82)	1.28 (1.27)	0.8629 (0.8653)	47.6 (45.9)	1.95 (1.83)	6.44 (6.77)	4.39
A2G (Trans.)	7.53 (7.27)	0.61 (0.61)	0.20 (0.16)	0.83 (0.84)	1.41 (1.40)	0.8753 (0.8764)	47.9 (46.8)	2.55 (2.41)	5.18 (5.37)	2.27

TABLE 6

Results after various editing of the latent DCT feature. S_A and I_R both have 128 DCT components. $S_A[N :] = 0$ means that we keep the lowest N components and manually set the remaining components to zero. See the accompanied video in our supplementary.

Method	Pos. $L_1 \downarrow$	Speed $L_1 \downarrow$	Acc. $L_1 \downarrow$	PCK \uparrow	STFT \downarrow	SSIM \uparrow	LPIPS \downarrow	FID \downarrow	Diversity \uparrow	Multimodality \uparrow
A2G [4]	7.86 (7.55)	0.67 (0.66)	0.24 (0.22)	0.81 (0.83)	1.13 (1.12)	0.8594 (0.8619)	48.6 (45.4)	2.22 (1.65)	6.58 (6.90)	4.10
A2G w/ DCT	8.22 (7.99)	0.68 (0.67)	0.25 (0.22)	0.80 (0.81)	1.17 (1.16)	0.8558 (0.8579)	50.4 (47.3)	1.58 (1.51)	8.01 (8.20)	4.27
$S_A[100 :] = 0$	8.23 (7.98)	0.68 (0.67)	0.25 (0.22)	0.80 (0.81)	1.17 (1.16)	0.8557 (0.8579)	51.1 (49.6)	1.61 (1.55)	8.00 (8.20)	4.29
$S_A[50 :] = 0$	8.24 (7.99)	0.68 (0.67)	0.25 (0.22)	0.79 (0.81)	1.15 (1.15)	0.8555 (0.8577)	51.6 (49.8)	1.58 (1.53)	8.02 (8.22)	4.28
$S_A[10 :] = 0$	8.95 (8.68)	0.70 (0.69)	0.23 (0.20)	0.77 (0.78)	1.12 (1.11)	0.8445 (0.8464)	51.4 (49.6)	2.23 (2.11)	8.46 (8.70)	6.15
$I_R[10 :] = 0$	8.24 (8.01)	0.68 (0.67)	0.25 (0.22)	0.79 (0.81)	1.16 (1.16)	0.8555 (0.8576)	51.4 (49.6)	1.61 (1.56)	8.01 (8.22)	4.27
$I_R[1 :] = 0$	8.24 (8.01)	0.68 (0.67)	0.25 (0.22)	0.79 (0.82)	1.16 (1.16)	0.8556 (0.8577)	51.4 (49.9)	1.62 (1.57)	8.02 (8.24)	4.25
$I_R = 0$	12.1 (12.1)	0.65 (0.65)	0.24 (0.24)	0.62 (0.62)	1.18 (1.18)	0.8432 (0.8432)	127.3 (127.3)	21.9 (21.9)	5.80 (5.80)	-

and V use separate learnable transformations and only one head is used. The following MLP of each transformer layer contains two FC layers, projecting the 16-dim feature to 256 and back to 16 (both using ReLU activation) for non-linear feature transformation. Similar to DanceRevolution [55], we apply a sliding window mask at the transformer encoders so that the gestures do not depend on the information that far from the current speech signal. The window size is set to 32, which is about 1.06 seconds. The sequence length at the training stage is set as 512 (*i.e.* 17.06 seconds).

They can all generate smooth motions through our visual inspection. The quantitative results are listed in Tab. 5. Using GRU as the backbone gives a similar similarity metric, where the Pos., PCK, STFT, and SSIM dropped but the Speed and Acc. improved. The transformer backbone gets a better similarity metric (*e.g.* Pos. L_1 , Speed L_1 , Acc. L_1 and PCK) but worse motion dynamics (*e.g.* STFT, Diversity, also see the supplemented video). The multimodality of the Transformer backbone is also worse than the TCN and GRU backbone. We notice the candy-wrapper effect of the elbow joints occasionally due to bad rotation configuration for the Transformer backbone.

6.3 Latent DCT space

Similar to MOJO [56], our latent codes could also be modeled in discrete cosine transform (DCT) space to support sampling per frequency band.

For example, we can insert a DCT right before the two FC layers predicting the mean and standard deviation (*i.e.* the latent space of a VAE) and insert an IDCT after them. With this modification, a sequence of time domain features is transformed to DCT coefficients (128 points in our experiments) and then back to the time domain, enabling frequency domain controls. In our experiments, we test inserting DCT and IDCT for both the shared feature and the motion-specific feature. But only the motion-specific branch adopts VAE while the shared feature branch adopts AE (*i.e.* only one FC layer) since we do not have paired motion and have to sample motion-specific code during inference.

Note that the encoders require fixed length input due to the extra length constraint posed by the DCT. So we split long test audio into fixed-length clips and extract all their latent features (time domain feature after IDCT) using the encoders in advance for this DCT variant. Then all the features are concatenated and then decoded to motions by the following TCN in a fully convolutional fashion as before.

In Tab. 6, we show the quantitative results of motions generated by editing the features in the DCT domain. The *Audio2Gestures w/ DCT* achieves similar performance with the original *Audio2Gestures* model. Then we test various frequency manipulation in the feature domain. Note that all the generated motions are still smooth (*i.e.* do not jitter) and valid (*i.e.* no invalid poses).

For audio-motion *shared code* S_A , all metrics gradually get worse as we drop (*i.e.* set to 0) the highest frequency bands of the audio features (see Tab. 6, middle) and only keeps the lowest {100, 50, 10} frequency bands, which indicates that the motions generated by *Audio2Gestures w/ DCT* are correlated with the input audio. We observe the generated motion is very slow after dropping too many high-frequency components, which, to some extent, shows the dynamic of the generated motion is well correlated to its audio control.

For *motion-specific code* I_R , only a few low-frequency bands (around 10) have an obvious influence on the final motion (see Tab. 6, bottom). This might be the result of that we encourage the audio-motion shared latent code to contain more information so that the input audio can control the generated motion effectively (see Sec. 4.2.1). But when we drop all the frequency bands ($I_R = 0$), all the metrics drop a lot, which means the motion specific-code is not degenerate and plays an important part in our formulation.

6.4 Application

We notice that motion-specific code extracted from a motion strongly controls the final motion output. To be specific, the synthesized motion is almost the same as the original motion used to extract this motion-specific code. This feature is



Fig. 7. Left: The generated motion is different from the reference motion because the motion-specific code is randomly sampled. Right: The generated motion is similar to the reference motion because the motion-specific code is extracted from the reference motion using the motion encoder.

perfect for a type of motion synthesis application where predefined motions are provided on the timeline as constraints. For example, if there is a n -frame long motion clip that we want the avatar to perform from frame t to $t + n$. We could extract its motion-specific code I_M with the motion encoder and directly replace the sampled motion-specific code I_R from t to $t + n$. Our model could generate a smooth motion from the edited motion-specific code. Please refer to our project page for the demonstration.

7 CONCLUSION

In this paper, we explicitly model the one-to-many mapping by splitting the latent code into shared code and motion-specific code. This simple solution with our customized training strategy effectively improves the similarity, diversity, and multimodality of the generated motion. We also demonstrate an application that the model could insert a specific motion into the generated motion by editing the motion-specific code, with smooth and realistic transitions. Despite the model could generate multimodal motions and provide users the ability to control the output motion, there exist some limitations. For example, the generated motion is not very related to what the person says. Future work could be improving the meaning of the generated motion by incorporating word embedding as an additional condition.

REFERENCES

- [1] Y. Ferstl and R. McDonnell, "Investigating the use of recurrent motion modelling for speech gesture generation," in *IVA '18 Proceedings of the 18th International Conference on Intelligent Virtual Agents*, Nov 2018. [Online]. Available: <https://trinityspeechgesture.scss.tcd.ie>
- [2] "Mixamo," <https://www.mixamo.com>, [Online; accessed 15-March-2021].
- [3] S. Ginosar, A. Bar, G. Kohavi, C. Chan, A. Owens, and J. Malik, "Learning individual styles of conversational gesture," in *CVPR*. IEEE, Jun. 2019.
- [4] J. Li, D. Kang, W. Pei, X. Zhe, Y. Zhang, Z. He, and L. Bao, "Audio2gestures: Generating diverse gestures from speech audio with conditional variational autoencoders," in *ICCV*, 2021.
- [5] S. Levine, C. Theobalt, and V. Koltun, "Real-Time Prosody-Driven Synthesis of Body Language," *ACM TOG*, vol. 28, no. 5, pp. 1–10, dec 2009. [Online]. Available: <https://dl.acm.org/doi/10.1145/1618452.1618518>
- [6] S. Levine, P. Krähenbühl, S. Thrun, and V. Koltun, "Gesture controllers," in *ACM SIGGRAPH 2010 papers*, 2010, pp. 1–11.
- [7] I. Habibie, M. Elgharib, K. Sarkar, A. Abdullah, S. Nyatsanga, M. Neff, and C. Theobalt, "A motion matching-based framework for controllable gesture synthesis from speech," in *SIGGRAPH 2022 Conference Proceedings*, 2022.
- [8] T. Ao, Q. Gao, Y. Lou, B. Chen, and L. Liu, "Rhythmic gesticulator: Rhythm-aware co-speech gesture synthesis with hierarchical neural embeddings," *ACM Transactions on Graphics (TOG)*, vol. 41, no. 6, pp. 1–19, 2022.
- [9] D. P. Kingma and M. Welling, "Auto-encoding variational bayes," *stat*, vol. 1050, p. 1, 2014.
- [10] I. Goodfellow, J. Pouget-Abadie, M. Mirza, B. Xu, D. Warde-Farley, S. Ozair, A. Courville, and Y. Bengio, "Generative adversarial nets," in *NeurIPS*, 2014, pp. 2672–2680.
- [11] X. Yan, A. Rastogi, R. Villegas, K. Sunkavalli, E. Shechtman, S. Hadap, E. Yumer, and H. Lee, "Mt-vae: Learning motion transformations to generate multimodal human dynamics," in *ECCV*, 2018, pp. 265–281.
- [12] A. Hernandez, J. Gall, and F. Moreno-Noguer, "Human motion prediction via spatio-temporal inpainting," in *ICCV*, 2019, pp. 7134–7143.
- [13] H. Y. Ling, F. Zinno, G. Cheng, and M. Van De Panne, "Character controllers using motion vae's," *ACM Trans. Graph.*, vol. 39, no. 4, Jul. 2020. [Online]. Available: <https://doi.org/10.1145/3386569.3392422>
- [14] E. Shlizerman, L. Dery, H. Schoen, and I. Kemelmacher-Shlizerman, "Audio to body dynamics," in *CVPR*, 2018.
- [15] X. Liu, Q. Wu, H. Zhou, Y. Xu, R. Qian, X. Lin, X. Zhou, W. Wu, B. Dai, and B. Zhou, "Learning hierarchical cross-modal association for co-speech gesture generation," in *2022 IEEE/CVF Conference on Computer Vision and Pattern Recognition (CVPR)*, 2022, pp. 10 452–10 462.
- [16] H. Liu, N. Iwamoto, Z. Zhu, Z. Li, Y. Zhou, E. Bozkurt, and B. Zheng, "DisCo: Disentangled implicit content and rhythm learning for diverse co-speech gestures synthesis," in *Proceedings of the 30th ACM International Conference on Multimedia*, ser. MM '22. New York, NY, USA: Association for Computing Machinery, 2022, p. 3764–3773. [Online]. Available: <https://doi.org/10.1145/3503161.3548400>
- [17] G. E. Henter, S. Alexanderson, and J. Beskow, "Moglow: Probabilistic and controllable motion synthesis using normalising flows," *ACM Trans. Graph.*, vol. 39, no. 6, Nov. 2020. [Online]. Available: <https://doi.org/10.1145/3414685.3417836>
- [18] D. P. Kingma and P. Dhariwal, "Glow: Generative flow with invertible 1x1 convolutions," in *NeurIPS*, 2018, pp. 10 215–10 224.
- [19] D. Pavillo, D. Grangier, and M. Auli, "Quaternet: A quaternion-based recurrent model for human motion," in *BMVC*, 2018.
- [20] K. Fragkiadaki, S. Levine, P. Felsen, and J. Malik, "Recurrent network models for human dynamics," in *ICCV*, 2015, pp. 4346–4354.
- [21] A. Jain, A. R. Zamir, S. Savarese, and A. Saxena, "Structural-rnn: Deep learning on spatio-temporal graphs," in *CVPR*, 2016, pp. 5308–5317.
- [22] J. Martinez, M. J. Black, and J. Romero, "On human motion prediction using recurrent neural networks," in *CVPR*, 2017, pp. 2891–2900.
- [23] X. Huang, M.-Y. Liu, S. Belongie, and J. Kautz, "Multimodal unsupervised image-to-image translation," in *ECCV*, 2018.
- [24] J.-Y. Zhu, R. Zhang, D. Pathak, T. Darrell, A. A. Efros, O. Wang, and E. Shechtman, "Toward multimodal image-to-image translation," in *NeurIPS*, I. Guyon, U. V. Luxburg, S. Bengio, H. Wallach, R. Fergus, S. Vishwanathan, and R. Garnett, Eds. Curran Associates, Inc., 2017,

- pp. 465–476. [Online]. Available: <http://papers.nips.cc/paper/6650-toward-multimodal-image-to-image-translation.pdf>
- [25] S. Tulyakov, M.-Y. Liu, X. Yang, and J. Kautz, “Mocogan: Decomposing motion and content for video generation,” in *CVPR*, 2018, pp. 1526–1535.
- [26] Y. Zhu, M. R. Min, A. Kadav, and H. P. Graf, “S3vae: Self-supervised sequential vae for representation disentanglement and data generation,” in *Proceedings of the IEEE/CVF Conference on Computer Vision and Pattern Recognition*, 2020, pp. 6538–6547.
- [27] A. B. L. Larsen, S. K. Sønderby, H. Larochelle, and O. Winther, “Autoencoding beyond pixels using a learned similarity metric,” ser. ICML’16. JMLR.org, 2016, p. 1558–1566.
- [28] X. Chen, Y. Duan, R. Houthoofd, J. Schulman, I. Sutskever, and P. Abbeel, “Infogan: Interpretable representation learning by information maximizing generative adversarial nets,” in *NeurIPS*, 2016, pp. 2172–2180.
- [29] J. Donahue, P. Krähenbühl, and T. Darrell, “Adversarial feature learning,” *arXiv preprint arXiv:1605.09782*, 2016.
- [30] Y. Zhou, C. Barnes, L. Jingwan, Y. Jimei, and L. Hao, “On the continuity of rotation representations in neural networks,” in *CVPR*, June 2019.
- [31] A. Defossez, G. Synnaeve, and Y. Adi, “Real time speech enhancement in the waveform domain,” *arXiv preprint arXiv:2006.12847*, 2020.
- [32] Z. Wang, A. C. Bovik, H. R. Sheikh, and E. P. Simoncelli, “Image quality assessment: from error visibility to structural similarity,” *IEEE TIP*, 2004.
- [33] R. Zhang, P. Isola, A. A. Efros, E. Shechtman, and O. Wang, “The unreasonable effectiveness of deep features as a perceptual metric,” in *CVPR*, 2018.
- [34] Y. Choi, Y. Uh, J. Yoo, and J.-W. Ha, “Stargan v2: Diverse image synthesis for multiple domains,” in *CVPR*, June 2020.
- [35] K. He, X. Zhang, S. Ren, and J. Sun, “Deep residual learning for image recognition,” in *CVPR*, 2016, pp. 770–778.
- [36] C. DOERSCH, “Tutorial on variational autoencoders,” *stat*, vol. 1050, p. 13, 2016.
- [37] Q. Mao, H.-Y. Lee, H.-Y. Tseng, S. Ma, and M.-H. Yang, “Mode seeking generative adversarial networks for diverse image synthesis,” in *CVPR*, 2019.
- [38] Z. Cao, T. Simon, S.-E. Wei, and Y. Sheikh, “Realtime multi-person 2d pose estimation using part affinity fields,” in *CVPR*, 2017, pp. 7291–7299.
- [39] M. Heusel, H. Ramsauer, T. Unterthiner, B. Nessler, and S. Hochreiter, “Gans trained by a two time-scale update rule converge to a local nash equilibrium,” in *NeurIPS*, 2017, pp. 6626–6637.
- [40] S. S. Stevens, J. Volkman, and E. B. Newman, “A scale for the measurement of the psychological magnitude pitch,” *The Journal of the Acoustical Society of America*, vol. 8, no. 3, pp. 185–190, 1937.
- [41] B. McFee, V. Lostanlen, A. Metsai, M. McVicar, S. Balke, C. Thomé, C. Raffel, F. Zalkow, A. Malek, Dana, K. Lee, O. Nieto, J. Mason, D. Ellis, E. Battenberg, S. Seyfarth, R. Yamamoto, K. Choi, viktorandreevichmorozov, J. Moore, R. Bittner, S. Hidaka, Z. Wei, nullmightybofo, D. Hereñú, F.-R. Stöter, P. Friesch, A. Weiss, M. Vollrath, and T. Kim, “librosa/librosa: 0.8.0,” Jul. 2020. [Online]. Available: <https://doi.org/10.5281/zenodo.3955228>
- [42] G. Pavlakos, V. Choutas, N. Ghorbani, T. Bolkart, A. A. A. Osman, D. Tzionas, and M. J. Black, “Expressive body capture: 3d hands, face, and body from a single image,” in *CVPR*, 2019.
- [43] A. Kanazawa, M. J. Black, D. W. Jacobs, and J. Malik, “End-to-End Recovery of Human Shape and Pose,” *CVPR*, pp. 7122–7131, 2018.
- [44] J. Zhang, P. Felsen, A. Kanazawa, and J. Malik, “Predicting 3D human dynamics from video,” in *ICCV*, vol. 2019-Octob, 2019, pp. 7113–7122. [Online]. Available: <https://jasonyzhang.com/phd>.
- [45] N. Kolotouros, G. Pavlakos, M. Black, and K. Daniilidis, “Learning to reconstruct 3D human pose and shape via model-fitting in the loop,” in *ICCV*, vol. 2019-Octob, 2019, pp. 2252–2261. [Online]. Available: <https://seas.upenn.edu/>
- [46] A. F. Agarap, “Deep learning using rectified linear units (relu),” *arXiv preprint arXiv:1803.08375*, 2018.
- [47] S. Bai, J. Z. Kolter, and V. Koltun, “An empirical evaluation of generic convolutional and recurrent networks for sequence modeling,” *arXiv preprint arXiv:1803.01271*, 2018.
- [48] X. Glorot and Y. Bengio, “Understanding the difficulty of training deep feedforward neural networks,” in *Proceedings of the Thirteenth International Conference on Artificial Intelligence and Statistics*, ser. Proceedings of Machine Learning Research, Y. W. Teh and M. Titterton, Eds., vol. 9. Chia Laguna Resort, Sardinia, Italy: PMLR, 13–15 May 2010, pp. 249–256.
- [49] D. P. Kingma and J. Ba, “Adam: A method for stochastic optimization,” in *ICLR*, 2015. [Online]. Available: <http://arxiv.org/abs/1412.6980>
- [50] A. Paszke, S. Gross, S. Chintala, G. Chanan, E. Yang, Z. DeVito, Z. Lin, A. Desmaison, L. Antiga, and A. Lerer, “Automatic differentiation in pytorch,” 2017.
- [51] S. Alexanderson, G. E. Henter, T. Kucherenko, and J. Beskow, “Style-controllable speech-driven gesture synthesis using normalising flows,” in *Computer Graphics Forum*, vol. 39, no. 2. Wiley Online Library, 2020, pp. 487–496.
- [52] I. Kobyzev, S. Prince, and M. Brubaker, “Normalizing flows: An introduction and review of current methods,” *IEEE TPAMI*, 2020.
- [53] K. Cho, B. van Merriënboer, Ç. Gülçehre, D. Bahdanau, F. Bougares, H. Schwenk, and Y. Bengio, “Learning phrase representations using rnn encoder-decoder for statistical machine translation,” in *EMNLP*, 2014.
- [54] A. Vaswani, N. Shazeer, N. Parmar, J. Uszkoreit, L. Jones, A. N. Gomez, u. Kaiser, and I. Polosukhin, “Attention is all you need,” in *NeurIPS*, ser. NIPS’17. Red Hook, NY, USA: Curran Associates Inc., 2017, p. 6000–6010.
- [55] R. Huang, H. Hu, W. Wu, K. Sawada, M. Zhang, and D. Jiang, “Dance revolution: Long-term dance generation with music via curriculum learning,” in *ICLR*, 2021. [Online]. Available: <https://openreview.net/forum?id=xGZG2kS5bFk>
- [56] Y. Zhang, M. J. Black, and S. Tang, “We are more than our joints: Predicting how 3d bodies move,” in *CVPR*, 2021, pp. 3372–3382.